


Preparation, characterization and application of phase-pure anatase and rutile TiO₂ nanoparticles by new green route

Edna R. Spada¹ · Eder A. Pereira² · Maykon A. Montanhera² · Leonardo H. Morais³ · Renato G. Freitas³ · Rodrigo G. F. Costa⁴ · Gabriela B. Soares⁴ · Caue Ribeiro⁴ · Fernando R. de Paula² 

Received: 31 May 2017 / Accepted: 28 July 2017 / Published online: 1 August 2017
© Springer Science+Business Media, LLC 2017

Abstract Titanium dioxide (TiO₂) is used in a range of applications such as photocatalysis and sensor devices. In this work, TiO₂ nanoparticles (TiO₂NPs) in the crystallographic forms anatase and rutile were prepared by the green route. The method involves dissolving titanium oxysulfate (TiOSO₄) powder in hydrogen peroxide (H₂O₂) solution and subsequent thermal treatment of the resultant amorphous precipitate. X-ray diffraction (XRD) was used to follow the structural evolution of the amorphous precipitate, and microstructure analysis was realized with Rietveld refinement. In addition, the photocatalytic activity of the synthesized TiO₂NPs was evaluated by studying the degradation of Rhodamine B (RhB) dye. The highest photocatalytic activity was observed for TiO₂ obtained at 600 °C in the crystallographic form anatase.

1 Introduction

Recently, TiO₂NPs have attracted attention due to their potential applications in pigments, photocatalysis, solar energy conversion, sensor devices, and antibacterial activities [1–5]. This wide range of applications is attributed to

some distinct properties of TiO₂, among which high redox potential, high chemical stability, low cost, and no toxicity stand out. These properties depend on many factors, such as the crystal structure, crystallite size, particle shape, and specific surface area, which are also strongly dependent on the method of synthesis. In terms of its crystal structure, TiO₂ exists as three important polymorphs: rutile (tetragonal), anatase (tetragonal), and brookite (orthorhombic) [6]. Rutile is the only stable phase; anatase and brookite are metastable at all temperatures and can be converted to rutile after heat treatment at high temperatures. Dependent on structure and particle size, each crystalline phase exhibits different physical properties best suited to different applications. For example, the anatase phase has a band gap of 3.2 eV, which means that it can be activated by UV light illumination. This is one of the reasons why it is often preferred for applications in photocatalysis [7–9]. The photocatalytic activity of TiO₂ originates from the presence of photo-generated electrons (e⁻) in the conduction band and holes (h⁺) in the valence band under irradiation with UV light. These holes have high oxidation power, thus they can easily react with adsorbed hydroxide ions to produce hydroxyl radicals, the main oxidizing species that are responsible for the photo-oxidation of organic compounds. The photocatalytic performance of anatase is considered superior to the more stable rutile (3.0 eV); this is attributed to a higher density of localized states and slower charge carrier recombination [10]. On the other hand, it has been reported that the presence of a small fraction of the rutile phase in intimate contact with anatase TiO₂ can improve its photocatalytic performance [11–13].

Pure anatase phase can be synthesized by many methods, such as the hydrothermal method, the sol gel method, the chemical method, and electrodeposition [14–19]. While all these methods have their own important benefits, the

✉ Fernando R. de Paula
depaula@dfq.feis.unesp.br

¹ Instituto de Física de São Carlos, Universidade de São Paulo – USP, São Paulo, SP, Brazil

² Faculdade de Engenharia, Universidade Estadual Paulista, Av. Brasil 56, Ilha Solteira, SP, Brazil

³ Departamento de Química, Universidade Federal de Mato Grosso, Cuiabá, MT 78060-900, Brazil

⁴ Embrapa Instrumentação, Rua Quinze de Novembro, 1452, São Carlos, SP 13560-970, Brazil

chemical method is one of the simplest and offers many advantages such as low cost, versatility, and the need for only simple equipment. Gao et al. [20] used aqueous peroxy-titanate solution at room temperature to deposit amorphous and nanometer sized TiO_2 thin films. Recently, Sankapal et al. reported large area deposition of TiO_2 on various substrates through the oxidation of TiOSO_4 by the H_2O_2 method [21].

In this work, TiO_2 nanoparticles in the anatase and rutile crystallographic forms were prepared by the aqueous route. The method involves dissolving TiOSO_4 powder in H_2O_2 solution and subsequent thermal treatment of the resultant amorphous precipitate. The structural properties of both as-prepared and annealed TiO_2 NPs were determined by XRD, and microstructure analysis was realized with Rietveld refinement. The surface morphology of the TiO_2 NPs was observed with a scanning electron microscope (SEM), and the photocatalytic activity of the samples was evaluated by monitoring the degradation of RhB in aqueous solution. The degradation of the dye was induced upon exposure to UV light in the presence of TiO_2 NPs.

2 Experimental procedure

2.1 Experimental section

2.1.1 Preparation

In the preparation of the titanium precursor, 0.02 mol L^{-1} of TiOSO_4 was dissolved in 2.50 mL of water at 10°C under vigorous magnetic stirring, and then after 30 min, 0.007 mol L^{-1} of H_2O_2 was added to the solution. A yellow colored acidic solution with a yellow precipitate was formed indicating the formation of peroxy-hydroxy titanium complexes. After this, the solution was transferred to a refrigerator and maintained at 5°C for 48 h. To remove impurities, e.g., SO_4^{2-} , the precipitate obtained was washed three times with water by vacuum filtration and dried at 60°C . Finally, the precipitate was annealed in air at different temperatures ranging from 400 to 1000°C for 4 h to obtain crystalline TiO_2 .

2.1.2 Materials characterization

The structures of the samples as-prepared as well as heat treated were studied by XRD at room temperature with a SHIMATZU XRD-6000 model, which provides $\text{Cu } K_\alpha$ radiation ($\lambda = 1.544 \text{ \AA}$). Measurements were taken in θ - 2θ configurations from 20° to 65° , with a step size of $0.2^\circ \text{ min}^{-1}$. Additionally, microstructure analysis, percentage of anatase and rutile, and average crystallite sizes were realized with Rietveld refinement as already

described by our research group elsewhere [22, 23]. A UV-Vis spectrophotometer (Varian Cary 100) with an integrating sphere attachment DRA-CA-30I for diffuse reflectance measurements was used to establish the optical band gap. Optical absorption was measured in the 200 – 800 nm range. SEM images were obtained with a ZEISS model EVO LS15 with acceleration voltage of 0.1 – 20 kV coupled with an EDX analyzer for stoichiometry. The photocatalytic activity of the samples for the oxidation of RhB was tested under UVC light illumination. The powders were placed in beakers and immersed in 20 mL of RhB aqueous solution (2.5 mg L^{-1}). The beakers were placed in a photo-reactor at 25°C and illuminated by six UVC lamps (TUV Philips, 15 W , with maximum intensity at 254 nm). All the tests were performed under vigorous stirring. The photocatalytic oxidation of RhB was monitored by taking UV-Vis measurements at various light exposure times.

3 Results and discussion

3.1 Thermal, stoichiometric, and morphological analysis

Figure 1a shows the thermogravimetry (TG) curve of the TiO_2 precursor after drying at 60°C for 2 h. The TG curve can roughly be divided into three stages. The first stage is from room temperature to 130°C where a mass loss of about 13% is observed, which can be attributed to the evaporation of physically adsorbed water. A mass loss of about 10% occurs in the temperature range of 130 – 350°C ; this is attributed to the thermal decomposition of the peroxy titanium complex. The amorphous precursor obtained was converted to the anatase phase as the temperature increased from 350 to 650°C . The anatase TiO_2 was transformed to the rutile phase between 650 and 1000°C . In order to investigate the composition of the as-prepared TiO_2 , EDX analysis was carried out on samples heated to 400 , 600 , 700 , 800 , 850 , 900 , and 1000°C . The chemical composition spectrum of the sample annealed at 600°C is shown in Fig. 1b: only titanium and oxygen elements were detected, and no impurities could be seen within the detection limits of EDX. The same result was obtained for all other samples including the as-prepared sample. The present composition of Ti and O guarantees the formation of stoichiometric TiO_2 .

Representative SEM images of the TiO_2 NPs samples are provided in Fig. 2. An overview of the powders at low magnification shows that the samples contain predominantly spherical agglomerates with some rod-like particles. Annealing at high temperatures did not cause significant changes in morphology, although according to

Fig. 1 **a** TG curve of TiO_2 precursor recorded in air at $3.0\text{ }^\circ\text{C min}^{-1}$ heating rate, **b** energy dispersive X-ray spectrometry (EDX) of TiO_2 sample annealing at $600\text{ }^\circ\text{C}$

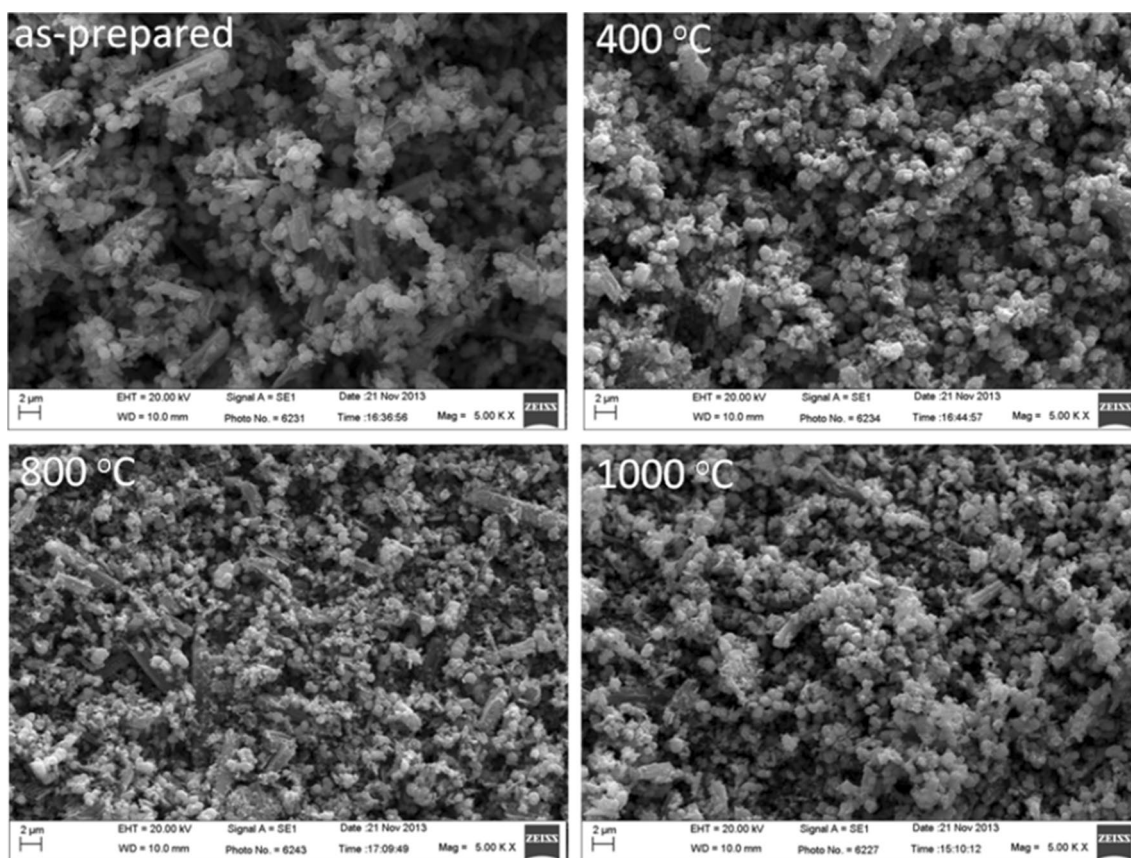
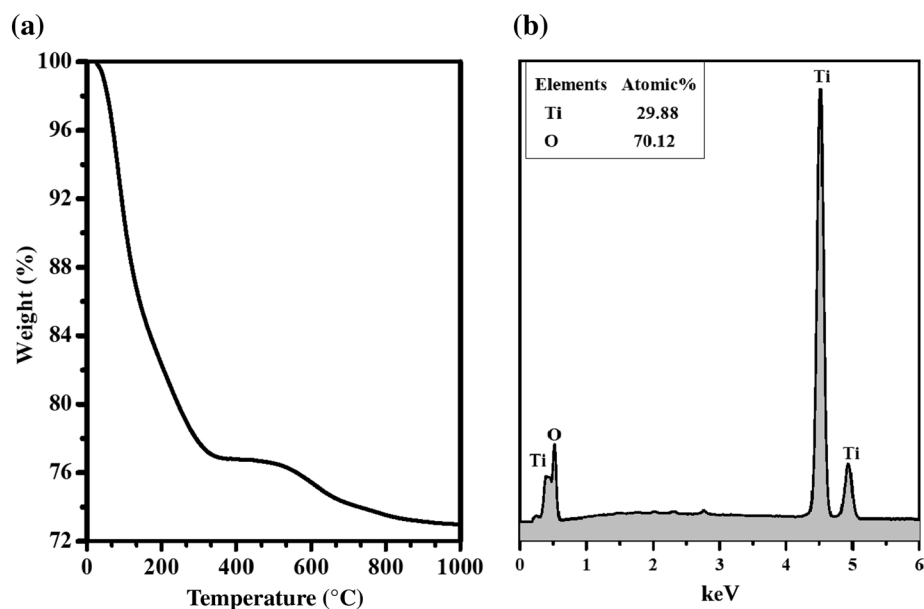


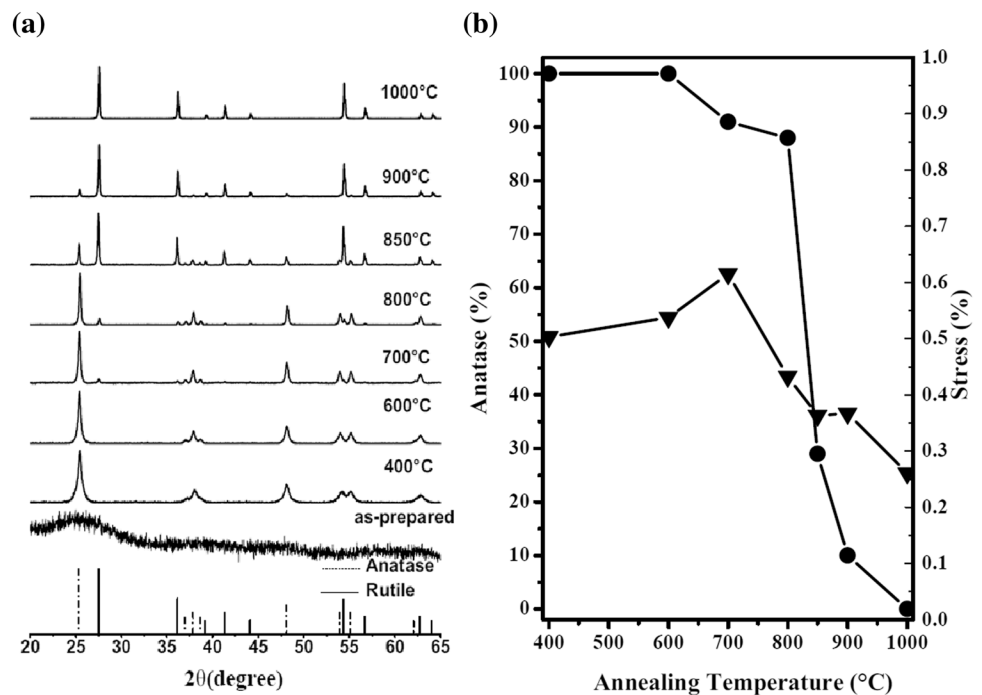
Fig. 2 The SEM micrographs of the morphology of TiO_2 NPs

the XRD data (shown in Fig. 3), we started out with an amorphous powder, obtaining pure anatase at $400\text{ }^\circ\text{C}$ followed by an anatase/rutile mixture at $800\text{ }^\circ\text{C}$; anatase was fully converted into rutile at $1000\text{ }^\circ\text{C}$.

3.2 Structure analysis

The powder XRD patterns of the as-prepared sample and samples annealed at 400, 600, 700, 800, 850, 900, and

Fig. 3 **a** XRD patterns of TiO₂ samples as-prepared and heated at 400, 600, 700, 800, 850, 900 and 1000 °C. **b** Variation in the proportion of anatase phase (filled circle) and stress (filled inverted triangle) at different annealing temperatures, 400, 600, 700, 800, 850, 900 and 1000 °C



1000 °C for 4 h are shown in Fig. 3a. The position of the peaks associated with anatase and rutile polymorphs was taken from ICDD 00-021-1272 and ICDD 01-076-0317, respectively. From the XRD pattern, it is observed that the as-prepared sample is amorphous. However, for annealing temperatures of 400 and 600 °C, the XRD pattern shows only the anatase phase; on the other hand, for 700 °C, the main content is the anatase phase with a modest amount of rutile (9%). With increase in annealing temperature, the most intense peak is observed at 27.5°; this is indicative of the presence of rutile phase. For the samples annealed at 850 and 900 °C, a small amount of remaining anatase is observed (30 and 10%, respectively); however at 1000 °C, only rutile phase is present. The full width at half maximum (FWHM) of the 101 diffraction peak of pure-phase anatase decreased with increasing annealing temperature suggesting that the average crystallite size increased through thermal treatment. In fact, the crystallite size estimated by Rietveld refinement for the samples annealed at 400 and 600 °C were 17 and 30 nm, respectively. For the pure-phase rutile obtained at 1000 °C, the average crystallite size was 57 nm. Figure 3b shows the variation in the proportion of anatase phase and the stress in the TiO₂ samples at different annealing temperatures obtained by Rietveld refinement. The TiO₂ sample obtained at 700 °C exhibits the highest stress whereas the sample obtained at 1000 °C has the lowest. The stress in the samples can be associated with the presence of oxygen defects at the grain boundary. In the sample treated at 700 °C, oxygen ions can be removed through the breaking of Ti–O bonds during the

processes of phase conversion from anatase to rutile, thus increasing the number of oxygen vacancies. However, some of these defects are removed with increasing temperature, which leads to a reduction of stress in the samples [24, 25].

3.3 UV–Vis spectra

In order to study the optical properties of the synthesized TiO₂NPs, their band gaps were investigated via UV–Vis diffuse reflectance spectra. Plots of $(ah\nu)^{0.5}$ versus E_g from UV–Vis spectrum data of the samples annealed at 600, 700, and 1000 °C are illustrated in Fig. 4. The bandgap energies E_g of the anatase and rutile phases were obtained by extrapolating the absorption edges to $\alpha=0$. The results obtained were 3.21 and 2.95 eV for the pure-phase anatase and rutile, respectively (see Fig. 4a). When the calcination temperature increases, the band gap decreases; these values are consistent with those obtained by Landmann et al. [26]. Compared to the pure-phase samples, the sample annealed at 700 °C presents two bandgap energies, 3.10 and 2.98 eV (see Fig. 4b). This occurs because the rutile phase does not exist as an overlayer on the surface of anatase particles, but exists separately from them [11].

3.4 Photocatalytic activity of TiO₂ particles

The effect of calcination temperature on the photocatalytic activity of TiO₂ was evaluated by RhB photodegradation. The analyses were performed on the samples annealed at 600, 700, and 1000 °C. In all cases, the samples were compared.

Fig. 4 Plots of $(\alpha h\nu)^{0.5}$ versus photon energy ($h\nu$): **a** samples annealed at 600 °C (pure anatase) and 1000 °C (pure rutile); **b** samples annealed at 700 °C (91% anatase 9% rutile)

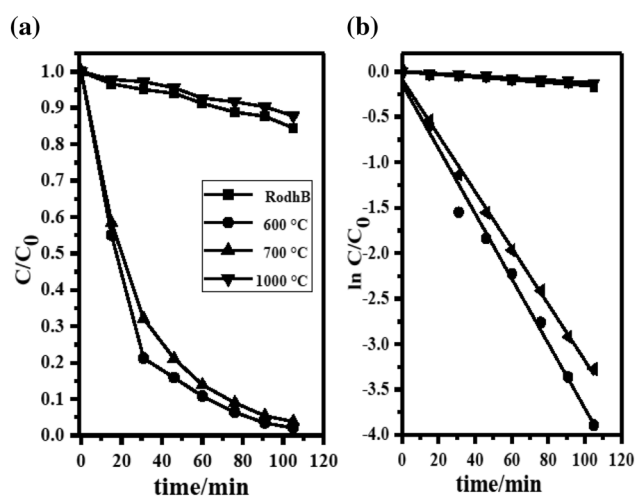
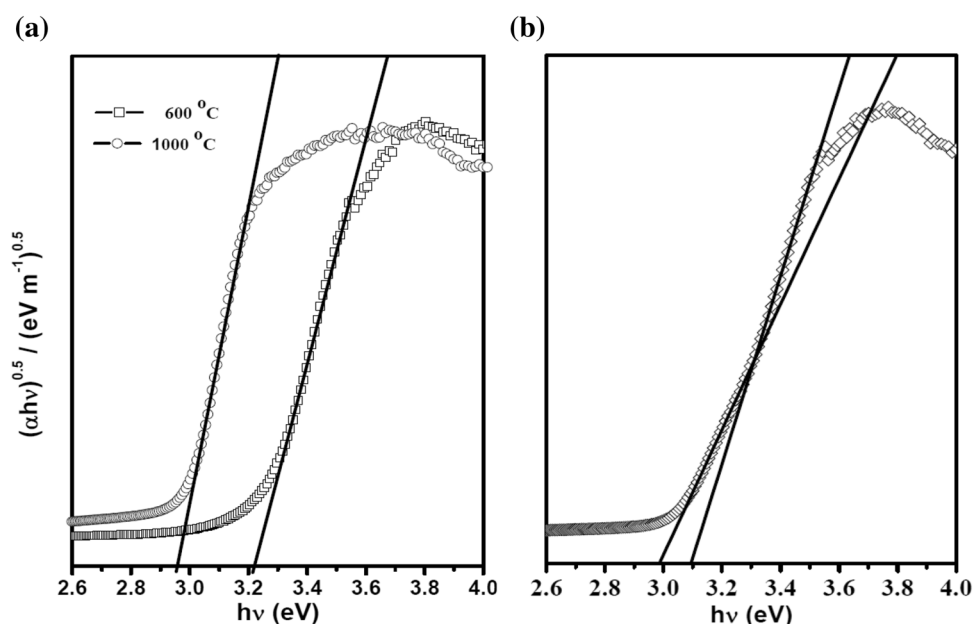


Fig. 5 Photodegradation profiles of the RhB solution, using TiO₂NPs with UVC light illumination. **a** Relationship between C/C_0 versus time irradiation **b** Relationship between $\ln C/C_0$ versus time irradiation

The photocatalytic performance of TiO₂NPs is presented in Fig. 5a for the photo-oxidation of RhB. From the photocatalytic efficiency plots of the different samples, the pseudo rate order of the photodegradation reaction was calculated in Fig. 5b. The reaction should be of pseudo first-order with respect to RhB, and must obey Eq. (1):

$$v = -\frac{d[\text{RhB}]}{dt} = k[\text{RhB}][\text{AS}] \quad (1)$$

where [AS] represents the photocatalyst's active sites on the catalyst's surface. As the same weight of catalysts was used in all the photocatalytic measurements, [AS] is considered constant over time and could be incorporated in the kinetic constant. By substituting $k'=k[\text{AS}]$ into Eq. (1) and integrating, we get Eq. (2), which could be useful for determining the kinetic constant:

$$\ln \frac{[\text{RhB}]}{[\text{RhB}]_0} = k't \quad (2)$$

A plot of $\ln C/C_0$ ($[\text{RhB}]/[\text{RhB}]_0$) as a function of t forms a straight line whose slope is k' , confirming the pseudo first-order reaction.

RhB photocatalytic degradation under UV-C illumination for TiO₂ synthesized materials presents similar behavior to other TiO₂ materials synthesized by different methods [27–30]. The photocatalytic degradation mechanism of RhB is influenced by a dye-sensitizing mechanism due to the color aspect of RhB, and this could generally increase effective degradation: as such its k' values are expected to be higher.

The results for the samples obtained at calcination temperatures of 600, 700, and 1000 °C indicate that with higher temperatures, photocatalytic activity (p.a.) becomes less effective; this is shown in Figs. 5 and 6, where the k' results are presented as column graphs.

The differences in p.a. performance of these samples are certainly influenced by changes in the number of active sites during the heat treatment. The number of active sites increases with the removal of organic residues from the surface and therefore the calcination

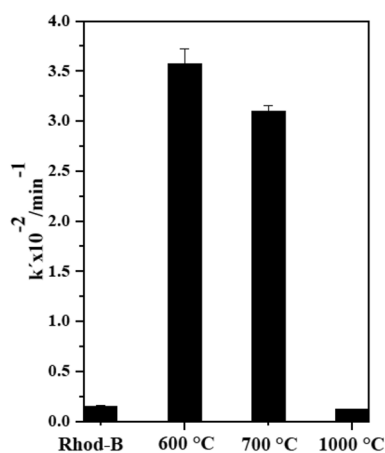


Fig. 6 Column graph of k' values under UVC illumination for RhB and with the addition of the TiO_2 NPs annealed at 600, 700, and 1000 °C

Table 1 Influence of calcination temperature on the crystalline structure and value kinetic constant of TiO_2 NPs

T (°C)	Crystallographic phase*	A (%)	k' ($10^{-2}/\text{min}^{-1}$)**
400	A	100	–
600	A	100	3.60
700	A/R	91	3.29
800	A/R	88	–
850	A/R	30	–
900	A/R	10	–
1000	R	0	0.12

*A and R denote the anatase and rutile, respectively

**Measured value of kinetic constant (k') of RhB pure ($0.15 \times 10^{-2}/\text{min}^{-1}$)

temperature influences these sites. The number of active sites is also influenced by the phase composition of TiO_2 . The calcination temperature changes the phase composition, especially the percentage of anatase, as previously presented by the XRD results (Fig. 3a). Anatase is the most studied TiO_2 phase, and it is well known for its superior catalytic activity when compared to rutile TiO_2 [10]. The p.a. of the sample annealed at 600 °C presents a superior value to the others, confirming that the principal influence of calcination temperature on the p.a. of the samples is mainly related to phase composition. The sample annealed at 700 °C presents p.a. similar to the sample annealed at 600 °C due to its phase composition being 91% anatase TiO_2 . However, the sample annealed at 1000 °C does not present p.a. as its behavior is very close to the photolysis of RhB without any catalysts as shown in Fig. 5. The same sample is composed only of rutile TiO_2 , confirming that this TiO_2 crystallographic

phase should not present p.a. As the crystal phase of the samples is modified by temperature, changes occur in the band gap value, these changes affect p.a. A summary of the results is shown in Table 1.

4 Conclusion

We conclude that the chemical route developed in this work is a promising low cost alternative for the preparation of phase pure anatase and rutile. XRD analysis showed that annealing at temperatures higher than 600 °C resulted in evident transformation of the anatase phase into rutile phase. The anatase phase decreases with an increase in the annealing temperature. Pure rutile phase was obtained by annealing nanostructured anatase at 1000 °C. The crystallite size increased from 17 to 57 nm with increase in the annealing temperature from 400 to 1000 °C. At the same time, the band gap values decreased from 3.21 to 2.93 eV. The photocatalytic degradation of RhB on these different phases was investigated. The highest photocatalytic activity was observed for TiO_2 NPs obtained at 600 °C, and the lowest was obtained for the sample obtained at 1000 °C.

Acknowledgements The authors thank the Brazilian agencies: CNPq (Universal 454704/2014-3-Scholarship process 152036/2016-4), FAPESP (Scholarship process 2011/11065-0), and the National Institute for Science and Technology on Organic Electronics (CNPq 573762/2008-2 and FAPESP 2008/57706-4) for financial support.

References

1. J. Papp, H.-S. Shen, R. Kershaw, K. Dwight, A. Wold, Titanium(IV) oxide photocatalysts with palladium. *Chem. Mater.* **5**, 284–288 (1993)
2. V. Guidi, M.C. Carotta, G. Martinelli, G. Sberveglieri, M. Ferroni, E. Comini, L. Paglialonga, Preparation of nanosized titania thick and thin films as gas-sensors. *Sens. Actuators B* **57**, 197–200 (1999)
3. X.Z. Ding, X.H. Liu, Correlation between anatase-to-rutile transformation and grain growth in nanocrystalline titania powders. *J. Mater. Res.* **13**, 2556–2559 (1998)
4. A. Sobhani-Nasab, Z. Zahrae, M. Akbari, M. Maddahfa, Synthesis, characterization, and antibacterial activities of $\text{ZnLaFe}_2\text{O}_4$. *J. Mol. Struct.* **1139**, 430–435 (2017)
5. M. Akbari, A. Aetemady, F. Firoozeh, M. Yaseliani, Synthesis of AgO-TiO_2 nanocomposite through a simple method and its antibacterial activities. *J. Mater. Sci.* **28**, 10245–10249 (2017)
6. M. Lazzeri, A. Vittadini, A. Selloni, Structure and energetics of stoichiometric TiO_2 anatase surfaces. *Phys. Rev. B* **63**, 155409–155417 (2001)
7. L. Wang, S.Z. Kang, X. Li, L. Qin, H. Yan, J. Mu, Rapid and efficient photocatalytic reduction of hexavalent chromium by using “water dispersible” TiO_2 nanoparticles. *Mater. Chem. Phys.* **178**, 190–195 (2016)
8. L. Ma, W. Xu, S. Zhu, Z. Cui, X. Yang, A. Inoue, Anatase TiO_2 hierarchical nanospheres with enhanced photocatalytic activity

- for degrading methyl orange. *Mater. Chem. Phys.* **170**, 186–192 (2016)
- S.M. Hosseinpour-Mashkani, A. Sobhani-Nasab, Green synthesis and characterization of NaEuTi₂O₆ nanoparticles and its photocatalyst application. *J. Mater. Sci.* **28**, 4345–4350 (2017)
 - K.E. Karakitsou, X.E. Verykios, Effects of altermultivalent cation doping of titania on its performance as a photocatalyst for water cleavage. *J. Phys. Chem.* **6**, 1184–1189 (1993)
 - A. Molinari, F. Bonino, G. Magnacca, F. Demaria, Relation between phase composition and photocatalytic activity of TiO₂ in a sulfoxide deoxygenation reaction. *Mater. Chem. Phys.* **158**, 60–66 (2015)
 - T. Ohno, K. Sarukawa, M. Matsumura, Photocatalytic activities of pure rutile particles isolated from TiO₂ powder by dissolving the anatase component in HF solution. *J. Phys. Chem. B* **105**, 2417–2420 (2001)
 - D.C. Hurum, A.G. Agrios, S.E. Crist, K.A. Gray, T. Rajh, M.C. Thurnauer, Probing reaction mechanisms in mixed phase TiO₂ by EPR. *J. Electron. Spectrosc. Relat. Phenom.* **150**, 155–163 (2006)
 - M. Andersson, L. Österlund, S. Ljungstroem, A. Palmqvist, Preparation of nanosize anatase and rutile TiO₂ by hydrothermal treatment of microemulsions and their activity for photocatalytic wet oxidation of phenol. *J. Phys. Chem. B* **106**, 10674–10679 (2002)
 - J.M. Wu, H.C. Shih, W.T. Wu, Electron field emission from single crystalline TiO₂ nanowires prepared by thermal evaporation. *Chem. Phys. Lett.* **413**, 490–494 (2005)
 - M.D. Blešić, Z. Šaponjić, J. Nedeljković, D. Uskoković, TiO₂ films prepared by ultrasonic spray pyrolysis of nanosize precursor. *Mater. Lett.* **54**, 298–302 (2002)
 - Y. Lei, L.D. Zhang, J.C. Fan, Fabrication, characterization and Raman study of TiO₂ nanowire arrays prepared by anodic oxidative hydrolysis of TiCl₃. *Chem. Phys. Lett.* **338**, 231–236 (2001)
 - A. Sobhani-Nasab, S.M. Hosseinpour-Mashkani, M. Salavati-Niasari, S. Bagheri, Controlled synthesis of CoTiO₃ nanostructures via two-step sol–gel method in the presence of 1,3,5-benzenetricarboxylic acid. *J. Cluster Sci.* **26**, 1305–1318 (2015)
 - L.F. Marchesi, R.G. Freitas, E.R. Spada, F.R. Paula, M.S. Góes, J.R. Garcia, Photoelectrochemical characterization of ITO/TiO₂ electrodes obtained by cathodic electrodeposition from aqueous solution. *J. Solid State Electrochem.* **19**, 2205–2211 (2015)
 - Y. Gao, Y. Masuda, Z. Peng, T. Yonezawa, K. Koumoto, Room temperature deposition of a TiO₂ thin film from aqueous peroxotitanate solution. *J. Mater. Chem.* **13**, 608–613 (2003)
 - B.R. Sankapal, M.C. Steiner, A. Ennaoui, Synthesis and characterization of anatase-TiO₂ thin films. *Appl. Surf. Sci.* **239**, 165–170 (2005)
 - R.G. Freitas, M.A. Santanna, E.C. Pereira, Dependence of TiO₂ nanotube microstructural and electronic properties on water splitting. *J. Power Sources* **251**, 178–186 (2014)
 - R.G. Freitas, F.W.S. Lucas, M.A. Santanna, R.A. Mendes, A.J. Terezo, G.L.C. de Souza, L.H. Mascaro, E.C. Pereira, An experimental and theoretical study on the electronic and structural properties of CdSe@TiO₂ nanotube arrays. *Phys. Chem. Chem. Phys.* **18**, 26885–26893 (2016)
 - N.H. Linha, T.Q. Nguyen, W.A. Diño, H. Kasai, Effect of oxygen vacancy on the adsorption of O₂ on anatase TiO₂(001): a DFT-based study. *Surf. Sci.* **633**, 38–45 (2014)
 - B. Choudhury, A. Choudhury, Local structure modification and phase transformation of TiO₂ nanoparticles initiated by oxygen defects, grain size, and annealing temperature. *Int. Nano Lett.* **3**, 55–63 (2013)
 - M. Landmann, E. Rauls, W.G. Schmidt, The electronic structure and optical response of rutile, anatase and brookite TiO₂. *J. Phys. Condens. Matter.* **24**, 195503–195508 (2012)
 - N. Serpone, E. Borgarello, R. Harris, P. Cahill, M. Borgarello, Photocatalysis over TiO₂ supported on a glass substrate. *Solar Energy Mater.* **14**, 121–127 (1986)
 - X. Zhang, M. Zhou, L. Lei, Preparation of anatase TiO₂ supported on alumina by different metal organic chemical vapor deposition methods. *Appl. Catal. A* **282**, 285–293 (2005)
 - G.B. Soares, B. Bravin, C.P.M. Vaz, C. Ribeiro, Facile synthesis of N-doped TiO₂ nanoparticles by a modified polymeric precursor method and its photocatalytic. *Appl. Catal. B* **106**, 287–294 (2011)
 - M. Dawson, G.B. Soares, C. Ribeiro, Preparation and photocatalytic performance of TiO₂:SiO₂ nanocomposites produced by the polymeric precursors method. *J. Nanosci. Nanotechnol.* **13**, 5126–5133 (2013)